Environmental Pollution 343 (2024) 123228

Contents lists available at ScienceDirect

Environmental Pollution

journal homepage: www.elsevier.com/locate/envpol

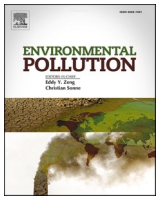

Atmospheric HONO emissions in China: Unraveling the spatiotemporal patterns and their key influencing factors☆

Cong Gan [a], Baojie Li [a,*], Jinyan Dong [a], Yan Li [a], Yongqi Zhao [a], Teng Wang [b], Yang Yang [a], Hong Liao [a]

[a] Collaborative Innovation Center of Atmospheric Environment and Equipment Technology, Jiangsu Key Laboratory of Atmospheric Environment Monitoring and Pollution Control, School of Environmental Science and Engineering, Nanjing University of Information Science & Technology, Nanjing, 210044, China
[b] College of Oceanography, Hohai University, Nanjing, 210098, China

ARTICLE INFO

Keywords:
HONO
Emission inventory
Fertilization
Spatiotemporal distribution

ABSTRACT

Nitrous acid (HONO) can be photolyzed to produce hydroxyl radicals (OH) in the atmosphere. OH plays a critical role in the formation of secondary pollutants like ozone (O_3) and secondary organic aerosols (SOA) via various oxidation reactions. Despite the abundance of recent HONO studies, research on national HONO emissions in China remains relatively limited. Therefore, this study employed a "wetting-drying" model and bottom-up approach to develop a high-resolution gridded inventory of HONO emissions for mainland China using multiple data. We used the Monte Carlo method to estimate the uncertainty in HONO emissions. In addition, the primary sources of HONO emissions were identified and their spatiotemporal distribution and main influencing factors were studied. The results indicated that the total HONO emissions in mainland China in 2016 were 0.77 Tg N (R_{50}: 0.28–1.42 Tg N), with soil (0.42 Tg N) and fertilization (0.26 Tg N) as the primary sources, jointly contributing to over 87% of the total. Notably, the North China Plain (NCP) had the highest HONO emission density (3.51 kg N/ha/yr). Seasonal HONO emissions followed the order: summer (0.38 kg N/ha) > spring (0.19 kg N/ha) > autumn (0.17 kg N/ha) > winter (0.06 kg N/ha). Moreover, HONO emissions were strongly correlated with fertilization, cropland, temperature, and precipitation. This study provides vital scientific groundwork for the atmospheric nitrogen cycle and the formation of secondary pollutants.

1. Introduction

The primary source of hydroxyl radicals (OH) in the troposphere, gaseous nitrous acid (HONO), has a considerable effect on atmospheric chemical processes (Liu et al., 2019; Sun et al., 2020; Xue et al., 2020). HONO photolysis can contribute more than 90% of atmospheric OH during haze pollution days (Zhang et al., 2022). The concentration of OH directly affects the atmospheric oxidative capacity (Yang et al., 2021). In the atmosphere, OH functions as a significant oxidant, which reacts with nitrogen oxides (NO_x) and volatile organic compounds (VOCs) (Wu et al., 2022), leading to the formation of ozone (O_3) (Zhang et al., 2016) and secondary organic aerosols (SOA) (Carlton et al., 2020; Zhang et al., 2019). Consequently, HONO has a significant influence on atmospheric photochemistry and local climate. (Wang et al., 2020). Currently, HONO sources fall into two main categories: direct emissions from sources including soil, traffic, and biomass burning, and secondary generation resulting from homogeneous and heterogeneous chemical reactions (Wu et al., 2022; Zhang et al., 2016, 2019). This study focuses on direct emissions of HONO.

The emission of HONO from soil is a consequence of both abiotic processes, such as NH_4^+ transformation to NO_2^-, and biotic processes, such as nitrification and denitrification by ammonia-oxidizing bacteria and archaea (Donaldson et al., 2014; Medinets et al., 2016; Weber et al., 2015), playing an important role in increasing HONO emissions in the atmosphere (Wu et al., 2019; Zhang et al., 2016). This contribution is particularly noteworthy in regions with extensive cropland (Xue et al., 2020). In addition, the use of nitrogen fertilizers increases the concentration of NH_4^+ during the nitrification process (Wang et al., 2021) and the abundance of functional genes of microorganisms (Di et al., 2014; Ouyang et al., 2018). Consequently, fertilization leads to additional HONO emissions from agricultural soils (Tang et al., 2019). It's worth highlighting that the agricultural nitrogen fertilizer consumption in

☆ This paper has been recommended for acceptance by Admir Créso Targino.
* Corresponding author.
E-mail address: baojieli@nuist.edu.cn (B. Li).

https://doi.org/10.1016/j.envpol.2023.123228
Received 26 September 2023; Received in revised form 22 December 2023; Accepted 23 December 2023
Available online 24 December 2023

China ranked first in the world (Wang et al., 2023). The widespread application of nitrogen fertilizers unavoidably exacerbates nitrogen emissions from agroecosystems and enhances HONO emissions, thus significantly affecting the nitrogen cycle (Wu et al., 2022).

Recently, researchers have conducted numerous observations to quantify soil HONO emissions. Soil HONO flux typically ranges from 20 to 3000 ng N/m^2/s, but significant uncertainties exist (Maljanen et al., 2013; Su et al., 2011). HONO emitted from soil can account for some of the missing HONO during the daytime (Meusel et al., 2018). Soil HONO emissions can reach levels of 1000 ng N/m^2/s when nitrogen fertilizers are applied to agricultural land (Xue et al., 2019). Despite quantification of soil HONO emissions from various land cover types (Bhattarai et al., 2018; Wu et al., 2019), fewer observation points result in substantial uncertainties. Consequently, the influence of soil HONO emissions on atmospheric pollutants in atmospheric models remains inadequately characterized.

Current research generally constructs a parameterized scheme by combining soil HONO emission flux and various influencing factors and then applies the scheme to regional air quality models to quantify the impact of HONO on atmospheric pollutants. For example, Wang et al. (2023) constructed a parameterization scheme of soil HONO emission fluxes with T and soil water content (SWC) and quantified the effect of soil HONO emissions on atmospheric HONO concentrations in combination with the CMAQ model. Wang et al. (2021) incorporated their parameterization scheme into the CMAQ model to quantify the impact of soil-emitted HONO on air quality after fertilization. Wu et al. (2022) conducted a more comprehensive assessment of global soil HONO emissions, but there may be uncertainties when applied to China. The above studies have focused mainly on soil HONO emissions, while others have studied source-specific or region-specific HONO emissions, for example, studies by Liao et al. (2021) on HONO emissions from traffic, Sun et al. (2020) on HONO emissions from ships, and Yin et al. (2023) on multi-source HONO emissions in Guangdong Province. This study considered more sources of HONO emissions and used more high-resolution data in mainland China.

Therefore, this study aimed to (1) develop a high-resolution HONO emission inventory for mainland China using the "wetting-drying" model and bottom-up approach; (2) identify the hot spots of each source of HONO emissions and analyze their spatiotemporal distribution characteristics; and (3) reveal the main factors influencing the HONO emissions. This study provides crucial scientific insights into the atmospheric nitrogen cycle and the reduction of secondary pollutant formation while also offering invaluable data support for improving the accuracy of regional air quality models (such as WRF-Chem and CMAQ).

2. Data and methods

2.1. Data sources

Fertilization data (B. Li et al., 2021; Zhao et al., 2023) were calculated based on data from MARA (2017) and NDRC (2017). We obtained daily precipitation information with a resolution of 0.1° × 0.1° from the NASA Global Precipitation Measurement (GPM) dataset (Huffman et al., 2019). Soil pH, cation exchange capacity (CEC), and organic carbon (OC) data were sourced from the Harmonized World Soil Database v 1.2 (http://www.fao.org/land-water/databases-and-software/hwsd/en/). Land cover type data were retrieved from Global surface coverage at a 30-m resolution in 2017 (Gong et al., 2019). China transportation network data were obtained from Open Street data (http://www.geofabrik.de). The refined cropland overfire area in each province was obtained by coupling two types of fire point remote sensing data, MCD64A1 and MCD14ML (Li et al., 2018).

2.2. HONO emissions

This study considered 16 sources of HONO emissions, including emissions from different soil cover types, fertilization, biomass burning, and traffic.

2.2.1. HONO emissions from soils

Current studies typically estimate soil HONO emissions by creating parameterized schemes with the assistance of meteorological models, such as WRF. The method relies on relatively few Chinese observations (Zhang et al., 2016, 2019), potentially introducing uncertainties when applied to China. Weber et al. (2015) found that field-based HONO emissions were similar to laboratory-measured emissions during the wetting-drying cycle. They combined HONO emissions during the wetting-drying cycle with biocrust composition and satellite data to estimate the field HONO emissions. Wu et al. (2022) utilized the "wetting-drying" method across different soil cover types for the estimation of global HONO emissions. Van Dijk et al. (2002) had shown that emissions obtained by this method are consistent with field measurements. The "wetting-drying" model does not rely on meteorological models and shows considerable potential for practical application (Weber et al., 2015). The "wetting-drying" model utilized easily accessible data and can be used for nationwide evaluation of soil HONO emissions.

The calculation of soil HONO emissions involved (1) direct soil HONO emissions: occurring with or without fertilization, and (2) soil HONO emissions due to fertilization: representing emissions post-fertilization that exclude direct soil emissions. Specifically, HONO emissions due to fertilization were calculated as the difference between HONO emissions from fertilized soil and unfertilized soil during the wetting-drying cycle (Wu et al., 2022). We used Equation (1) to compute the total direct HONO emissions and fertilizer-induced HONO emissions from soil in China ($E_{CS,HONO}$, Tg N/yr)

$$E_{CS,HONO} = \left(E_{CR} + E_{FR} + E_{GL} + E_{SL} + E_{WL} + E_{BL} + E_{fer}\right) * CRF \quad (1)$$

where E_{CR}, E_{FR}, E_{GL}, E_{SL}, E_{WL}, and E_{BL} represent the direct HONO emissions from cropland, forest, grassland, shrubland, wetland, and bare land, respectively. E_{fer} represents HONO emissions induced by fertilization. Studies indicate that plant canopies may affect the emission of HONO through various mechanisms, such as uptake and deposition (Meng et al., 2022; Sörgel et al., 2011). This study corrected these effects through the canopy reduction factor (CRF) to avoid significantly overestimating soil HONO emissions in forest regions. The CRF formula is represented by Equation (2):

$$\mathrm{CRF} = \left(\frac{e^{-(k_a * \mathrm{SAI})} + e^{-(k_b * \mathrm{LAI})}}{2}\right) \quad (2)$$

where k_a and k_b are the plant leaf uptake constants, fixed at 8.75 and 0.24 (Yienger and Levy, 1995). Leaf area index (LAI) was acquired from the global monitoring data of NOAA. Our LAI data are resolved daily, thus addressing the problem of coarse resolution in previous studies (Wu et al., 2022). Stomatal area index (SAI) was computed using LAI/SAI values across various land cover types, as detailed by Yienger and Levy (1995).

As for direct soil HONO emissions, this study considered six land cover types, including cropland, forest, grassland, shrubland, wetland, and bare land (Gong et al., 2019). For the different land cover types, we calculated their HONO emissions ($E_{LC,cell}$ kg N/ha/yr) induced by precipitation and temperature for each grid cell separately (Equation (3)).

$$E_{LC,cell} = E_{HONO,int,LC} * P_{cell} * T_{cell} \quad (3)$$

where $E_{HONO,int,LC}$ is the mean HONO emissions for each land-cover type during a wetting and drying cycle (Table S1). P_{cell} indicates the count of monthly precipitation events per grid cell. An episode of precipitation is characterized by daily rainfall of more than 0.1 mm at the central location. T_{cell} stands for the calibration coefficient for temperature, which can be computed using Equation (4):

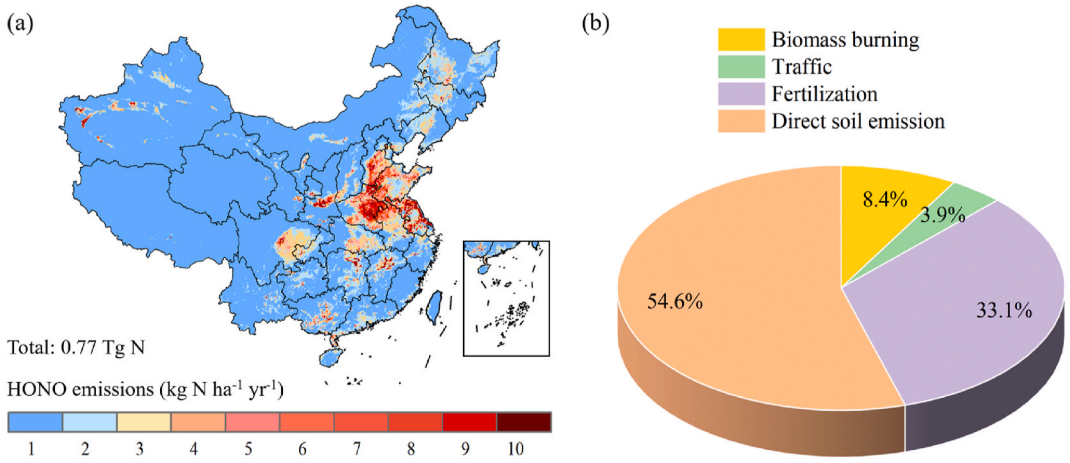

Fig. 1. (a) Spatial distribution of HONO emission density, and (b) share of each source.

$$T_{cell} = e^{0.103*T} / (Q_{10} * 2.5) \quad (4)$$

where T represents the temperature (°C) of the monthly mean soil surface (Muñoz Sabater, 2019), and the Q_{10} value is averaged using the soil HONO flux data at varying temperatures sourced from Oswald et al. (2013). Additionally, a calibration constant of 2.5 is used for soil temperature (Wu et al., 2022).

2.2.2. HONO emissions from fertilization

The increase in the abundance of functional genes of microorganisms due to fertilization, leading to the emission of HONO, represents a substantial source that deserves attention (Xue et al., 2021). The current studies commonly employ parameterized schemes to estimate HONO emissions from fertilization (Song et al., 2023; Wang et al., 2021). However, these parameterization schemes vary, primarily due to differences in the selected regions, time, and sample size. In our study, we employed high-resolution monthly fertilization data to calculate HONO emissions ($E_{fer,\ cell}$, kg N/ha/month) from fertilization within each grid cell using Equation (5):

$$E_{fer,cell} = F_{cell} * EF \quad (5)$$

where F_{cell} represents the fertilizer input (kg N/ha/month) for different grid cells, and EF denotes the emission factor (%) due to fertilization. The EF values were computed using Equation (6) (Wu et al., 2022). We verified the accuracy of Equation (6) by comparing the uncertainty range (R_{50}) of the calculated emission factors (EFs) with the observed values (Table S4).

$$EF = 3 * 10^{-5} * {Q_{fer}}^2 - 0.003 * Q_{fer} + 0.1 \quad (6)$$

where Q_{fer} represents fertilizer usage (kg N/ha).

2.2.3. HONO emissions from other sources

Tunnel tests have been proven more effective in obtaining the levels of traffic-related HONO emissions and accurately reflecting actual operating conditions (Gentner and Xiong, 2017). Several studies have revealed that traffic represents a notable origin of HONO emissions using HONO/NO_x ratios ranging from 0.29% to 1.7% (Kurtenbach et al., 2001; Xu et al., 2015). We used a HONO/NO_x ratio of 1.31 to estimate HONO emissions from traffic (S. Li et al., 2021). The NO_x emission data were sourced from the Tsinghua University MEIC inventory (Li et al., 2017).

Biomass burning is another contributor to atmospheric HONO. Some researchers estimate HONO emissions from biomass burning using the HONO/CO ratio (Veres et al., 2010; Wu et al., 2022). We calculated HONO emissions from biomass burning using the amount of biomass burning and emission factors, as shown in Equation (7):

$$E_{HONO,BB} = (A_{FB} + A_{HB} + A_{HF} + A_{FF}) * EF \quad (7)$$

where $E_{HONO,BB}$ is the estimated HONO emissions from biomass burning, and A_{FB}, A_{HB}, A_{HF}, and A_{FF} refer to activity data for field straw burning (including rice, corn, and wheat), household straw burning (including rice, corn, and wheat), household firewood, and forest fire, respectively. Activity data were obtained directly from statistical yearbooks (NBS – National Bureau of Statistics, 2017). EF represents the emission factor for each biomass-burning species (Cui et al., 2021).

2.3. Factors influencing HONO emissions

We used Spearman's rank correlation coefficient to explore the correlation between HONO emissions and the amount of fertilizer applied, soil pH, cation exchange capacity (CEC), organic carbon (OC), the percentage of each land cover type, transportation network density, the amount of biomass burning, precipitation, temperature, and wind speed. This analysis aimed to identify the primary factors influencing HONO emissions. Soil physical and chemical properties and land-cover types displayed relatively minor temporal variations at the grid cell level, and fertilization exhibited a nonlinear trend. Consequently, we computed correlations between fertilization, physico-chemical properties of soil, land cover types, and HONO emissions with a spatial resolution of 5′ × 5′ (roughly 10 × 10 km). The monthly-scale analysis of the relationship between HONO emissions and meteorological variables, including temperature, precipitation, and wind speed, is conducted for each grid.

2.4. Uncertainty analysis

Employing the Monte Carlo simulation approach, we evaluated the inconclusiveness of HONO emissions. This method has been extensively used in various inventory studies (Kang et al., 2016; Li et al., 2019; Rabbani et al., 2019). We assumed that the uncertainties in the activity levels and emission factors (EFs) followed a normal distribution. The coefficient variation (CV) of fertilization activity levels was derived from (Huang et al., 2012). Uncertainties in EFs for HONO emissions from soils were estimated by fitting sample data sourced from different literature. Activity levels and emission factors for biomass burning uncertainties were obtained from Shen et al. (2013) and Cui et al. (2021). Other factors, such as the share of each land-cover type, LAI, soil temperature, and wind speed exhibited relatively small fluctuations (details in Table S5). The HONO emissions calculations underwent 10,000 repetitions, with all inputs randomly selected. R_{50} values (the difference between the 75th and 25th quartiles) were used to characterize the

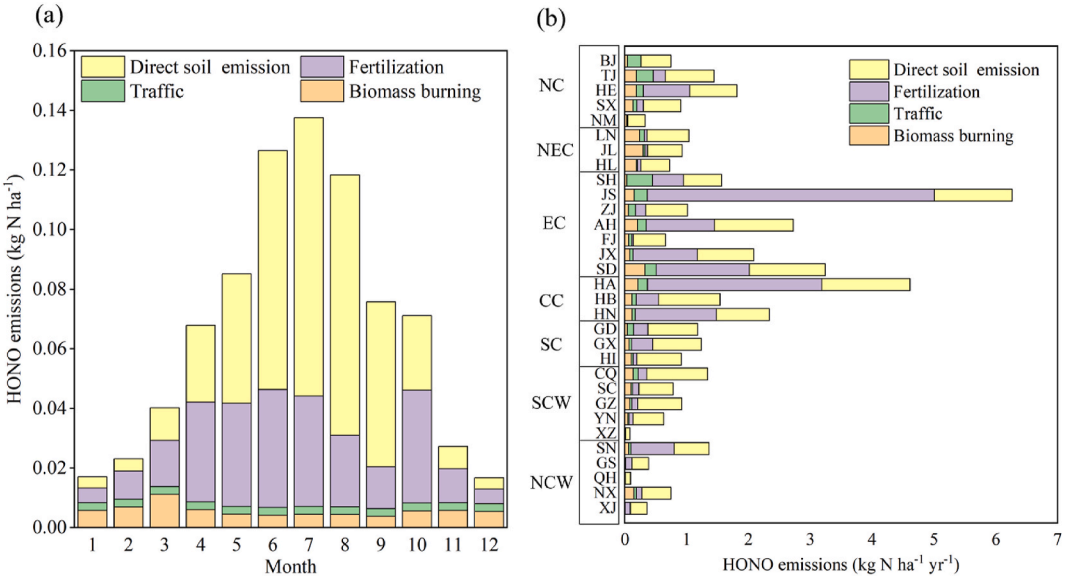

Fig. 2. (a) Monthly HONO emission density of each source, and (b) HONO emission density of each source in each province. Where NC, NEC, EC, CC, SC, SCW, and NCW represent North China, Northeast China, East China, Central China, South China, Southwest China, and Northwest China, respectively.

uncertainties.

3. Results and discussion

3.1. Emission estimation and comparison

The total HONO emissions in mainland China in 2016 were 0.77 (R_{50}: 0.28–1.42) Tg N (Fig. 1a). The primary contributors to these emissions were soil and fertilization, accounting for 54.6% (0.42 Tg N with a range from 0.16 to 0.67 Tg N) and 33.1% (0.26 Tg N with a range from 0.07 to 0.61 Tg N) of the total, respectively. It highlights the significant role of anthropogenic activities in HONO emissions. Biomass burning contributed 65.3 Gg N, followed by forests at 56.9 Gg N, grasslands at 36.6 Gg N, traffic at 30.0 Gg N, and bare land at 28.5 Gg N. HONO emissions from wetlands and shrublands each contributed less than 1%.

Our study found that the total soil HONO emissions were 0.68 (R_{50}: 0.23–1.28) Tg N in 2016, consistent with the 0.58 Tg discovered in 2017 (Wu et al., 2022). We estimated HONO emissions from fertilization (0.20 Tg N) in China based on the methodology of Song et al. (2023), which aligns with the emissions (0.26 Tg N) in this study. The mean HONO soil flux ranged from −0.86 to 20.25 ng N/m^2/s as measured by Tang et al. (2019), while our estimated value was 10.79 ± 12.25 ng N/m^2/s at the same location. Wang et al. (2021) reported HONO emission fluxes of 0–350 ng N/m^2/s from soils located in the NCP using a dynamic chamber system, compared to our estimation of 11.44 ± 12.48 ng N/m^2/s. Song et al. (2020) reported HONO emission fluxes of 0–5.9 ng N/m^2/s from soils in the eastern part of Chongming Island, while our calculation was 1.77 ± 1.54 ng N/m^2/s. Our estimates were in general agreement with the values reported in other studies (Table S3).

3.2. Spatiotemporal distribution of HONO emissions

There is a significant seasonal variation in HONO emissions in China, with augmented levels observed in the summer, in contrast to reduced levels detected in winter. HONO emissions were highest in July, reaching 0.14 kg N/ha (17.1%). Meanwhile, emissions in October and April were reported at 0.07 kg N/ha (8.8%) and 0.07 kg N/ha (8.4%), respectively. Notably, January recorded the lowest HONO emissions of 0.02 kg N/ha, representing only 2.1% of the annual emissions (Fig. 2a). Specifically, HONO emissions in July were approximately 8 times higher than those in January. Previous research has shown that HONO emissions from agricultural soils significantly contribute to the elevation of atmospheric O_3 levels (Xue et al., 2021). More specifically, Wang et al. (2021) reported a 5–6 ppb rise in O_3 in certain locations in the North China Plain (NCP) around noon after applying about 80 ng N/m^2/s HONO flux from fertilized soil to the CMAQ model. Similarly, inducing HONO emissions from cropland that exceeded 100 ng N/m^2/s to a 3D chemical transport model (such as the Chemistry and Weather Research and Forecasting model) led to a rise of 2.4–3.6 ppb of O_3 in eastern China (Zhang et al., 2016). China experiences elevated ozone levels during the summer, and HONO probably plays a significant role in ozone formation.

Table 1
HONO emission density of each source in seven regions of China.

Regions	Sources				
	Direct soil emission	Fertilization	Traffic	Biomass burning	Sum
CC	1.08	1.45	0.09	015	2.77
EC	1.00	1.35	0.13	0.16	2.63
NC	0.37	0.11	0.03	0.06	0.57
NCW	0.25	0.11	0.01	0.01	0.37
NEC	0.52	0.05	0.03	0.22	0.83
SC	0.79	0.28	0.06	0.06	1.19
SCW	0.32	0.04	0.05	0.05	0.42

Note: The unit in this table is “kg N/ha/yr”.

The HONO emission density in China was 0.81 kg N/ha/yr. Twenty provinces had HONO emission densities above the national mean, including Jiangsu, Henan, and Shandong provinces, which were among the top three in China with 6.27, 4.61, and 3.24 kg N/ha/yr, respectively, well above the national mean (Fig. 2b). HONO emissions, excluding fertilization, in these three provinces were 1.72 ± 0.07 kg N/ha/yr, exhibiting minimal differences. Differences in HONO emissions resulting from fertilization were observed in Jiangsu, Henan, and Shandong provinces, with respective amounts of 4.64, 2.82, and 1.50 kg N/ha/yr, highlighting the role of fertilization in provinces with high emissions. We conducted Pearson correlation analysis between total HONO emissions and each source. The result revealed a strong positive correlation of total HONO emissions with emissions from fertilization ($r = 0.96$) and weaker positive correlations with emissions from direct soil emissions ($r = 0.47$), traffic ($r = 0.31$), and biomass burning ($r = 0.27$).

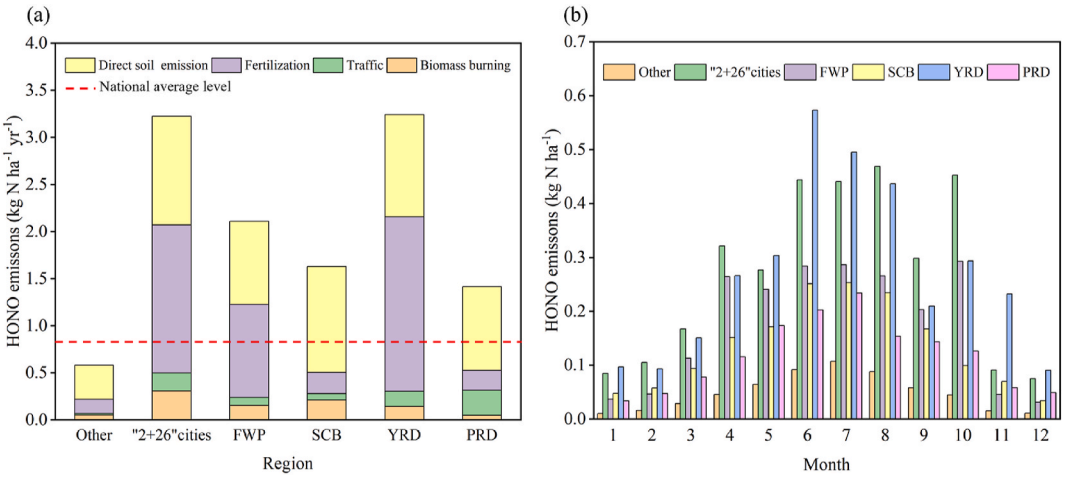

Fig. 3. (a) Annual HONO emission density in the O_3 pollution focus area, and (b) monthly HONO emission density in the O_3 pollution focus area.

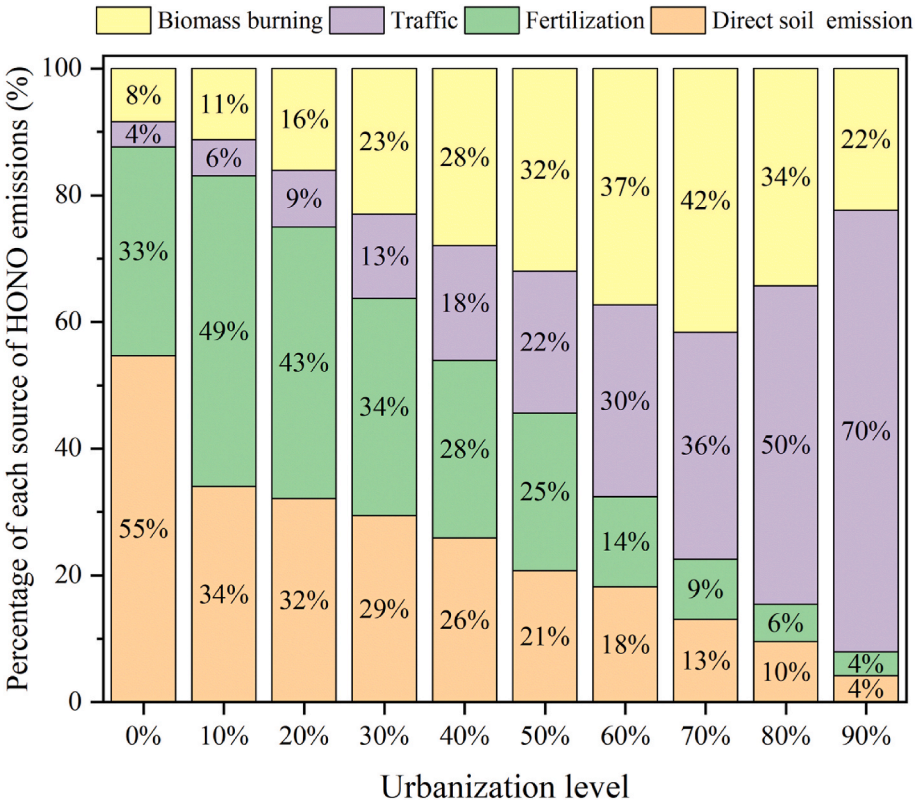

Fig. 4. Percentage of each source of HONO emissions as urbanization increases. Urbanization is quantified as the proportion of impervious surface within each 5′ × 5′ grid.

We conducted a comparison of HONO emissions in seven regions of China. Our analysis revealed that Central China (CC) (2.77 kg N/ha/yr), East China (EC) (2.63 kg N/ha/yr), and South China (SC) (1.19 kg N/ha/yr) had higher HONO emissions than the other regions (Table 1), which exhibited emissions below the national mean (0.81 kg N/ha/yr). Notably, the share of cropland in the Central China (CC) region reached 31.1%, which far exceeded the national mean (14.2%), and nitrogen fertilization in the East China (EC) region was 12.42 kg/km^2, which was 3.53 times higher than the national mean (3.52 kg/km^2) (NBS – National Bureau of Statistics, 2017). The higher HONO emissions in these regions were closely associated with their higher proportion of cropland and large amounts of nitrogen fertilization. Interestingly, even though Northeast China (NEC) has a significant portion of cropland (35.1%) and high nitrogen fertilization (5.77 kg/km^2), HONO emissions remained relatively low. This difference comes from the region's high latitude and low temperatures, which limit HONO emissions.

3.2.1. *HONO emissions in O_3-polluted focal areas*

Fenwei Plain (FWP), 2 + 26 cities, Sichuan Basin (SCB), Yangtze River Delta (YRD), and Pearl River Delta (PRD) regions have been found to have high atmospheric O_3 concentrations in China (Jin and Holloway, 2015; McLachlan et al., 2018; Wu and Xie, 2017). Therefore, we analyzed HONO emissions in these areas to understand their contribution to O_3 formation. Our findings reveal that the annual mean of HONO emissions in the 2 + 26 cities, FWP, SCB, YRD, PRD, and the rest were 3.23, 2.11, 1.63, 3.24, 1.41, and 0.58 kg N/ha/yr, respectively (Fig. 3a).

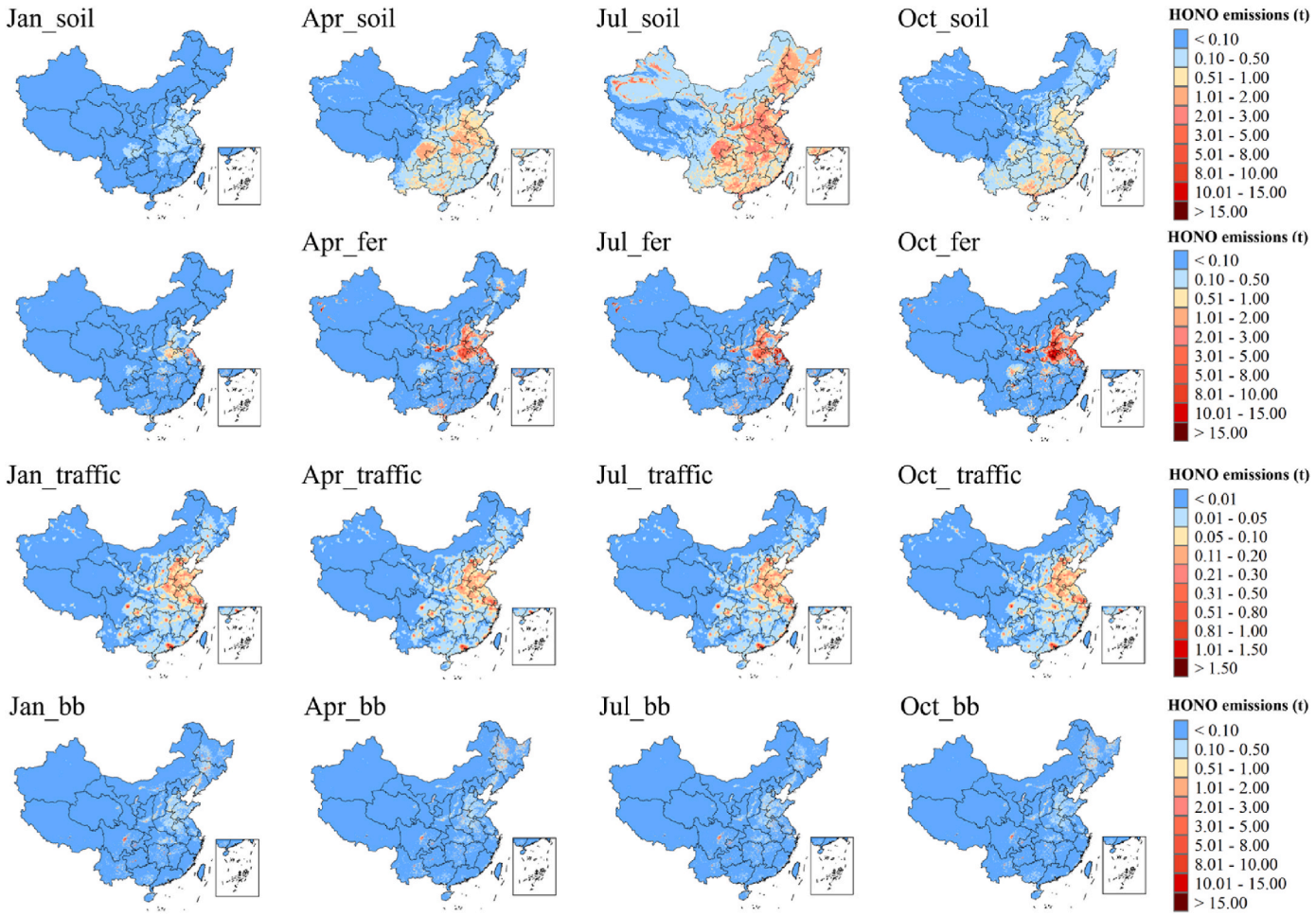

Fig. 5. Spatial distribution of HONO emissions from soil (first row), fertilization (second row), traffic (third row) and biomass burning (fourth row) in January, April, July, and October 2016.

Notably, these regions with high O_3 concentrations exhibited significantly greater HONO emission capacities compared to other areas. In particular, in 2 + 26 cities and YRD, HONO emission density was 5.57 and 5.59 times higher than in other regions. Photolysis of more HONO can lead to more OH radicals, which enhances atmospheric oxidation and thus increases the risk of O_3 pollution. Throughout the year, the HONO emission density in the 2 + 26 cities and YRD regions consistently exceeded that in other regions, thus getting designated as "perennially high HONO emission" regions (Fig. 3b). Consequently, for future studies on HONO, including air quality modeling and field observations, prioritizing the 2 + 26 cities and Yangtze River Delta regions is recommended. Furthermore, both HONO emission density and total HONO emissions in the five primary O_3 high-pollution zones exhibit significant seasonal variation, with peaks in summer and troughs in winter (Fig. 2a and 3b). Hence, summer should be the focal season for HONO research.

We further analyzed the sources and characteristics of urban HONO emissions on a national scale. As urbanization increased, we observed a notable shift in the composition of HONO emissions. The percentage of direct soil HONO emissions gradually decreased from 55% to 4% (Fig. 4). Concurrently, the share of fertilizer-induced HONO emissions also exhibited a decreasing trend, declining from 33% to 4% (Fig. 4). This decline in soil HONO emissions can be attributed to the proportional decrease in cropland and forests as impervious surfaces increase. In contrast, HONO emissions from traffic showed a significant rise from 4% to 70% (Fig. 4), emphasizing the prominence of traffic-related HONO emissions in highly urbanized areas. Additionally, HONO emissions from biomass burning constitute 42% of total emissions at an urbanization level of 70%, showing a decreasing trend thereafter (Fig. 4).

3.2.2. *Spatiotemporal distribution of HONO emissions from each source*

Since soil emissions account for up to 87.7% of total HONO emissions, this study focused on the spatiotemporal distribution of direct soil emissions and fertilizer-induced HONO emissions for in-depth analysis. In China, direct soil emissions exhibit a seasonal pattern, peaking in July at 93.37 g N/ha, followed by April and October at 25.80 g N/ha and 25.02 g N/ha, while January records the lowest emission at 3.69 g N/ha (Fig. 5). The mean soil surface (0–7 cm) temperature in summer in China after gridding was 7.38 °C, which was significantly higher than the 3.14 °C, 3.20 °C, and −0.97 °C in spring, fall, and winter (Muñoz Sabater, 2019). Summer also experienced frequent wetting-drying cycles (13.81 times in summer, 7.77 times in spring, 9.62 times in fall, and 4.53 times in winter) (Huffman et al., 2019). These environmental conditions in summer, characterized by higher temperatures and alternating wetting-drying periods, can induce HONO emissions (Wu et al., 2022). In spatial terms, the NCP, Central China, and SCB regions are HONO emissions hotspots because of their higher proportion of cropland. For example, Henan (49.0%), Sichuan (36.7%), and Hebei (34.6%) are 3.45, 2.58, and 2.43 times higher than the national mean (14.2%), respectively (NBS – National Bureau of Statistics, 2017).

The distribution of HONO emissions from fertilization in China differs from that of direct soil HONO emissions. In particular, emissions of 33.46 g N/ha (12.5%), 37.10 g N/ha (13.9%), and 37.94 g N/ha (14.2%) were recorded in April, July, and October, respectively, whereas lower

Table 2
Correlations and P-value of HONO emissions and influencing factors in China.

Influencing factors	Correlation (ρ)	Significance (P)
Fertilization	0.87	<0.01
pH	0.21	<0.01
CEC	−0.04	<0.01
OC	−0.17	<0.01
Cropland	0.88	<0.01
Forest	−0.02	<0.01
Grassland	−0.49	<0.01
Shrubland	0.04	<0.01
Wetland	0.00	>0.01
Bare land	−0.17	<0.01
Impervious surface	0.64	<0.01
Transportation network density	0.41	<0.01
Amount of biomass burning	0.55	<0.01

emissions of 5.01 g N/ha (only 1.9%) occurred in January. In the North China Plain, the extensive utilization of N fertilizers was the primary cause of the higher HONO emissions. For example, Jiangsu (18.56 kg N/km^2) and Henan (17.25 kg N/km^2) exceeded the national mean (3.52 kg N/km^2) by 4.27 and 3.90 times, respectively (NBS – National Bureau of Statistics, 2017).

HONO emissions resulting from traffic were relatively low and mainly located in NCP, YRD, and PRD regions, as illustrated in Fig. 5. Monthly variations in HONO emissions from traffic were not significant. HONO emissions resulting from biomass burning activities were mainly located in NC, NEC, and SCW regions (Fig. 5). HONO emissions from biomass burning activities peaked at 11.14 g N/ha in March. In other months, HONO emissions were 5.17 ± 0.91 g N/ha. Thus, the seasonality of HONO emissions primarily results from seasonal variations in soil HONO emissions.

3.3. Key influencing factors of HONO emissions

Spatial analysis revealed a notable positive relationship (correlation coefficient ρ = 0.87; P < 0.01) between HONO emissions and the amount of N fertilizer used, and a similar correlation of 0.88 (P < 0.01) was found between HONO emissions and cropland (Table 2). Fertilization and direct soil emissions emerge as the primary sources of HONO emissions, with the higher correlation coefficients observed between HONO emissions and these two factors. There are minimal correlations between HONO emissions and soil physicochemical properties or land-cover types other than cropland. In addition, we observed that soil pH exerts an influence on HONO emissions at the national scale (ρ = 0.21; P < 0.01), which aligns with a prior study conducted in Shanghai, reporting a correlation between maximum HONO fluxes and soil pH (ρ = 0.17) (Wu et al., 2022). Other research supports the findings that the favorable conditions for microbial growth as soil pH increases result in higher HONO emissions (Ermel et al., 2018). The correlation coefficients between HONO emissions and impervious surfaces, transportation network density, and biomass burning were above 0.4 (Table 2).

A statistically significant positive correlation between HONO emissions and temperature was discovered in the temporal analysis, with a coefficient of 0.89 (P < 0.01) (Fig. 6b and e). Additionally, precipitation also showed a high correlation with HONO emissions (ρ = 0.71; P < 0.01) (Fig. 6a and d). In this study, temperature and precipitation were crucial indicators for assessing HONO emissions and thus explaining their significant correlations with HONO emissions. Nevertheless, the dispersion of HONO relies primarily on the airflow movement. A negative relationship between wind speed and HONO emissions was observed (ρ = −0.25; P < 0.01) (Fig. 6c and f). Overall, HONO emissions are mainly positively affected by fertilization, cropland percentage, temperature, and precipitation and negatively affected by wind speed.

3.4. Uncertainty in HONO emissions

We performed 10,000 Monte Carlo simulations to evaluate the uncertainty regarding the difference between the 75th and 25th quartiles. In 2016, China exhibited direct HONO emissions varying between 0.28

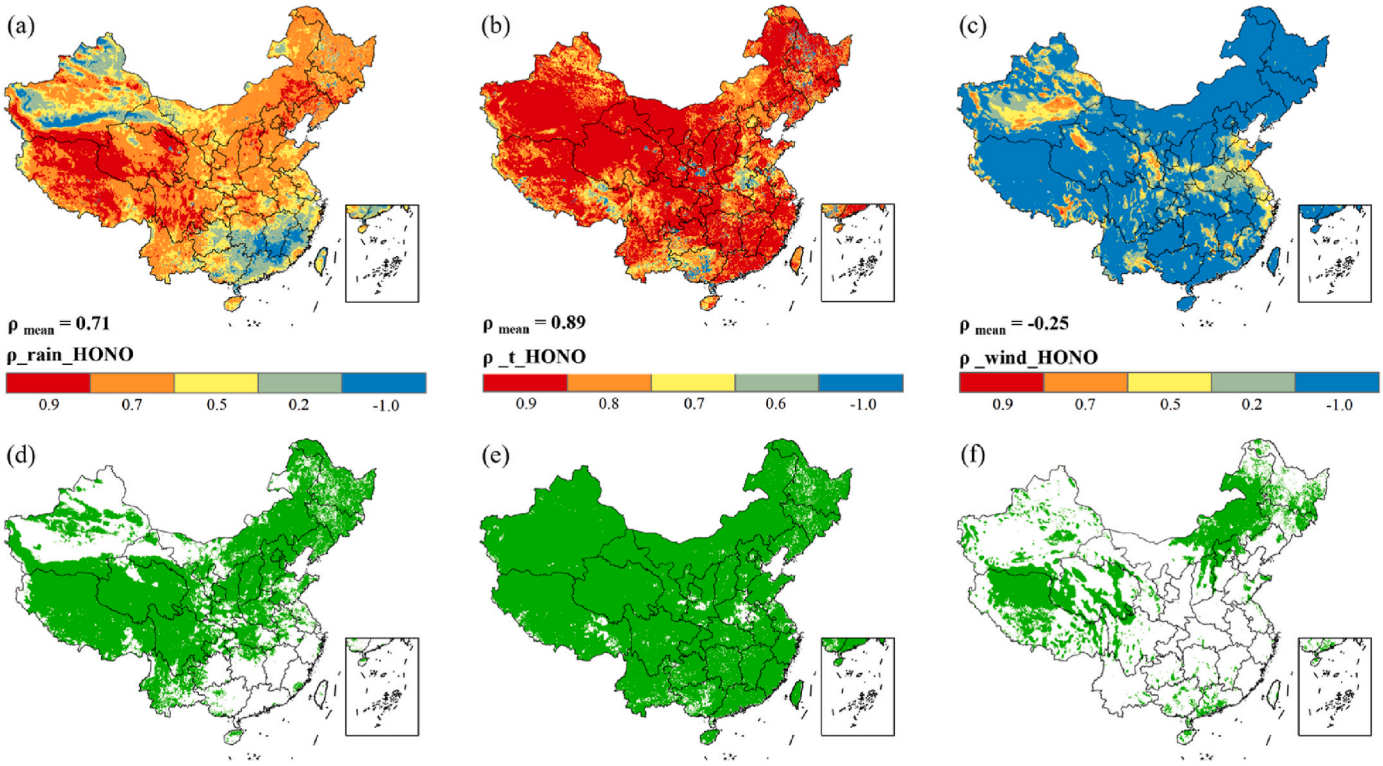

Fig. 6. Correlations and point distributions with P < 0.01 between HONO emissions and precipitation (a, d), temperature (b, e), and wind speed (c, f) on monthly time scales.

and 1.42 Tg N. Specifically, soil HONO emissions ranged from 0.16 to 0.67 Tg N, and HONO emissions from fertilization covered a range of 0.07–0.61 Tg N. Soil and fertilization were the main sources of HONO emissions and uncertainty in total emissions primarily arose from these two sources. The uncertainty in fertilization surpassed that in direct soil emissions, with the emission factor being the largest contributor to the uncertainty in fertilizer-induced HONO emissions. Future efforts will prioritize more comprehensive field observations to reduce uncertainty in emission factors, particularly those for HONO emissions resulting from fertilization. The estimated ranges for HONO emissions from traffic and biomass burning were 0.02–0.04 Tg N and 0.03–0.09 Tg N, respectively, showing relatively lower uncertainty. These two sources generated lower HONO emissions, consequently contributing less to the uncertainty of total HONO emissions.

4. Conclusion

This study employed the "wetting-drying" model and bottom-up approach to establish the high-resolution gridded HONO emission inventory of mainland China. We considered currently more comprehensive HONO emission sources at a national scale. Consistent with other studies, direct soil emissions accounted for the largest share of HONO emissions. However, fertilization (33.1%), a factor often overlooked in previous research, emerged as the second-largest source of HONO emissions. HONO emissions reached their peak in July and dropped to the lowest levels in January. Spearman's analysis revealed that fertilization, cropland, temperature, and precipitation significantly influenced HONO emissions.

We considered almost all sources of HONO emissions, but there are still some limitations. Firstly, the current emission inventories might have some uncertainties, primarily due to the limited research on emission factors in previous studies. Secondly, there may be unidentified sources of HONO, necessitating further investigation into HONO emissions. Thirdly, the study did not account for the secondary generation of HONO, which requires further refinement for future work. We believe that the high-resolution inventory of HONO emissions presented in this study establishes a scientific basis for the formulation of atmospheric policies and improvements in air quality.

CRediT authorship contribution statement

Cong Gan: Conceptualization, Data curation, Methodology, Software, Writing - original draft. **Baojie Li:** Conceptualization, Resources, Supervision, Writing - review & editing. **Jinyan Dong:** Resources. **Yan Li:** Resources. **Yongqi Zhao:** Resources. **Teng Wang:** Data curation. **Yang Yang:** Supervision. **Hong Liao:** Supervision.

Declaration of competing interest

The authors declare that they have no known competing financial interests or personal relationships that could have appeared to influence the work reported in this paper.

Data availability

Data will be made available on request.

Acknowledgements

This research has been supported by the National Natural Science Foundation of China [Grant 42021004], the National Natural Science Foundation of China [Grant 42377393 and 42107385], and the Natural Science Foundation of Jiangsu Province [Grant BK20220031]. HONO emission data are available on the Zenodo website (https://zenodo.org/records/10084466).

Appendix A. Supplementary data

Supplementary data to this article can be found online at https://doi.org/10.1016/j.envpol.2023.123228.

References

Bhattarai, H.R., Virkajärvi, P., Yli-Pirilä, P., Maljanen, M., 2018. Emissions of atmospherically important nitrous acid (HONO) gas from northern grassland soil increases in the presence of nitrite (NO_2^-). Agric. Ecosyst. Environ. 256, 194–199. https://doi.org/10.1016/j.agee.2018.01.017.

Carlton, A.G., Christiansen, A.E., Flesch, M.M., Hennigan, C.J., Sareen, N., 2020. Multiphase atmospheric chemistry in liquid water: impacts and controllability of organic aerosol. Acc. Chem. Res. 53, 1715–1723. https://doi.org/10.1021/acs.accounts.0c00301.

Cui, L., Li, R., Fu, H., Meng, Y., Zhao, Y., Li, Q., Chen, J., 2021. Nitrous acid emission from open burning of major crop residues in mainland China. Atmos. Environ. 244, 117950 https://doi.org/10.1016/j.atmosenv.2020.117950.

Di, H.J., Cameron, K.C., Podolyan, A., Robinson, A., 2014. Effect of soil moisture status and a nitrification inhibitor, dicyandiamide, on ammonia oxidizer and denitrifier growth and nitrous oxide emissions in a grassland soil. Soil Biol. Biochem. 73, 59–68. https://doi.org/10.1016/j.soilbio.2014.02.011.

Donaldson, M.A., Bish, D.L., Raff, J.D., 2014. Soil surface acidity plays a determining role in the atmospheric-terrestrial exchange of nitrous acid. Proc. Natl. Acad. Sci. U.S.A. 111, 18472–18477. https://doi.org/10.1073/pnas.1418545112.

Ermel, M., Behrendt, T., Oswald, R., Derstroff, B., Wu, D., Hohlmann, S., Stönner, C., Pommerening-Röser, A., Könneke, M., Williams, J., Meixner, F.X., Andreae, M.O., Trebs, I., Sörgel, M., 2018. Hydroxylamine released by nitrifying microorganisms is a precursor for HONO emission from drying soils. Sci. Rep. 8, 1877. https://doi.org/10.1038/s41598-018-20170-1.

Gentner, D.R., Xiong, F., 2017. Tracking pollutant emissions. Nat. Geosci. 10, 883–884. https://doi.org/10.1038/s41561-017-0027-y.

Gong, P., Liu, H., Zhang, M., Li, C., Wang, J., Huang, H., Clinton, N., Ji, L., Li, Wenyu, Bai, Y., Chen, B., Xu, B., Zhu, Z., Yuan, C., Ping Suen, H., Guo, J., Xu, N., Li, Weijia, Zhao, Y., Yang, J., Yu, C., Wang, X., Fu, H., Yu, L., Dronova, I., Hui, F., Cheng, X., Shi, X., Xiao, F., Liu, Q., Song, L., 2019. Stable classification with limited sample: transferring a 30-m resolution sample set collected in 2015 to mapping 10-m resolution global land cover in 2017. Sci. Bull. 64, 3. https://doi.org/10.1016/j.scib.2019.03.002.

Huang, X., Song, Y., Li, M., Li, J., Huo, Q., Cai, X., Zhu, T., Hu, M., Zhang, H., 2012. A high-resolution ammonia emission inventory in China. Global Biogeochem. Cycles 26. https://doi.org/10.1029/2011GB004161, 2011GB004161.

Huffman, J.G., Stocker, F.E., Bolvin, T.D., Nelkin, J., E, J.T., 2019. GPM IMERG late precipitation L3 1 day 0.1 degree x 0.1 degree V06. In: Savtchenko, A., Greenbelt, M. (Eds.), Goddard Earth Sciences Data and Information Services Center (GES DISC). NASA Goddard Space Flight Center. https://doi.org/10.5067/GPM/IMERGDL/DAY/06.

Jin, X., Holloway, T., 2015. Spatial and temporal variability of ozone sensitivity over China observed from the Ozone Monitoring Instrument: ozone sensitivity over China. J. Geophys. Res. Atmos. 120, 7229–7246. https://doi.org/10.1002/2015JD023250.

Kang, Y., Liu, M., Song, Y., Huang, X., Yao, H., Cai, X., Zhang, H., Kang, L., Liu, X., Yan, X., He, H., Zhang, Q., Shao, M., Zhu, T., 2016. High-resolution ammonia emissions inventories in China from 1980 to 2012. Atmos. Chem. Phys. 16, 2043–2058. https://doi.org/10.5194/acp-16-2043-2016.

Kurtenbach, R., Becker, K.H., Gomes, J.A.G., Kleffmann, J., Lörzer, J.C., Spittler, M., Wiesen, P., Ackermann, R., Geyer, A., Platt, U., 2001. Investigations of emissions and heterogeneous formation of HONO in a road traffic tunnel. Atmos. Environ. 35, 3385–3394. https://doi.org/10.1016/S1352-2310(01)00138-8.

Li, B., Chen, L., Shen, W., Jin, J., Wang, T., Wang, P., Yang, Y., Liao, H., 2021. Improved gridded ammonia emission inventory in China. Atmos. Chem. Phys. 21, 15883–15900. https://doi.org/10.5194/acp-21-15883-2021.

Li, B., Wang, J., Wu, S., Jia, Z., Li, Y., Wang, T., Zhou, S., 2019. New method for improving spatial allocation accuracy of industrial energy consumption and implications for polycyclic aromatic hydrocarbon emissions in China. Environ. Sci. Technol. 53, 4326–4334. https://doi.org/10.1021/acs.est.8b06915.

Li, B., Zhou, S., Wang, T., Sui, X., Jia, Z., Li, Y., Wang, J., Wu, S., 2018. An improved gridded polycyclic aromatic hydrocarbon emission inventory for the lower reaches of the Yangtze River Delta region from 2001 to 2015 using satellite data. J. Hazard Mater. 360, 329–339. https://doi.org/10.1016/j.jhazmat.2018.08.011.

Li, M., Liu, H., Geng, G., Hong, C., Liu, F., Song, Y., Tong, D., Zheng, B., Cui, H., Man, H., Zhang, Q., He, K., 2017. Anthropogenic emission inventories in China: a review. Natl. Sci. Rev. 4, 834–866. https://doi.org/10.1093/nsr/nwx150.

Li, S., Song, W., Zhan, H., Zhang, Y., Zhang, X., Li, W., Tong, S., Pei, C., Wang, Y., Chen, Y., Huang, Z., Zhang, R., Zhu, M., Fang, H., Wu, Z., Wang, J., Luo, S., Fu, X., Xiao, S., Huang, X., Zeng, J., Zhang, H., Chen, D., Gligorovski, S., Ge, M., George, C., Wang, X., 2021. Contribution of vehicle emission and NO_2 surface conversion to nitrous acid (HONO) in urban environments: implications from tests in a tunnel. Environ. Sci. Technol. 55, 15616–15624. https://doi.org/10.1021/acs.est.1c00405.

Liao, S., Zhang, J., Yu, F., Zhu, M., Liu, J., Ou, J., Dong, H., Sha, Q., Zhong, Z., Xie, Y., Luo, H., Zhang, L., Zheng, J., 2021. High gaseous nitrous acid (HONO) emissions from light-duty diesel vehicles. Environ. Sci. Technol. 55, 200–208. https://doi.org/10.1021/acs.est.0c05599.

Liu, Y., Lu, K., Li, X., Dong, H., Tan, Z., Wang, H., Zou, Q., Wu, Y., Zeng, L., Hu, M., Min, K.-E., Kecorius, S., Wiedensohler, A., Zhang, Y., 2019. A comprehensive model

test of the HONO sources constrained to field measurements at rural North China Plain. Environ. Sci. Technol. 53, 3517–3525. https://doi.org/10.1021/acs.est.8b06367.

Maljanen, M., Yli-Pirilä, P., Hytönen, J., Joutsensaari, J., Martikainen, P.J., 2013. Acidic northern soils as sources of atmospheric nitrous acid (HONO). Soil Biol. Biochem. 67, 94–97. https://doi.org/10.1016/j.soilbio.2013.08.013.

MARA, 2017. Ministry of Agriculture and Rural Affairs of China: China Animal Husbandry and Veterinary Yearbook. China Agriculture Press.

McLachlan, M.S., Undeman, E., Zhao, F., MacLeod, M., 2018. Predicting global scale exposure of humans to PCB 153 from historical emissions. Environ. Sci.: Process. Impacts 20, 747–756. https://doi.org/10.1039/C8EM00023A.

Medinets, S., Gasche, R., Skiba, U., Medinets, V., Butterbach-Bahl, K., 2016. The impact of management and climate on soil nitric oxide fluxes from arable land in the Southern Ukraine. Atmos. Environ. 137, 113–126. https://doi.org/10.1016/j.atmosenv.2016.04.032.

Meng, F., Qin, M., Fang, W., Duan, J., Tang, K., Zhang, H., Shao, D., Liao, Z., Feng, Y., Huang, Y., Ni, T., Xie, P., Liu, J., Liu, W., 2022. Measurement of HONO flux using the aerodynamic gradient method over an agricultural field in the Huaihe River Basin, China. J. Environ. Sci. 114, 297–307. https://doi.org/10.1016/j.jes.2021.09.005.

Meusel, H., Tamm, A., Kuhn, U., Wu, D., Leifke, A.L., Fiedler, S., Ruckteschler, N., Yordanova, P., Lang-Yona, N., Pöhlker, M., Lelieveld, J., Hoffmann, T., Pöschl, U., Su, H., Weber, B., Cheng, Y., 2018. Emission of nitrous acid from soil and biological soil crusts represents an important source of HONO in the remote atmosphere in Cyprus. Atmos. Chem. Phys. 18, 799–813. https://doi.org/10.5194/acp-18-799-2018.

Muñoz Sabater, J., 2019. ERA5-Land Monthly Averaged Data from 1981 to Present. https://doi.org/10.24381/cds.e2161bac.

NBS – National Bureau of Statistics, 2017. China Statistical Yearbook 2016. China Statistics Press.

NDRC, 2017. National development and reform commission of China. In: National Data on the Cost and Profit of Agricultural Product 2016. China Market Press.

Oswald, R., Behrendt, T., Ermel, M., Wu, D., Su, H., Cheng, Y., Breuninger, C., Moravek, A., Mougin, E., Delon, C., Loubet, B., Pommerening-Röser, A., Sörgel, M., Pöschl, U., Hoffmann, T., Andreae, M.O., Meixner, F.X., Trebs, I., 2013. HONO emissions from soil bacteria as a major source of atmospheric reactive nitrogen. Science 341, 1233–1235. https://doi.org/10.1126/science.1242266.

Ouyang, Y., Evans, S.E., Friesen, M.L., Tiemann, L.K., 2018. Effect of nitrogen fertilization on the abundance of nitrogen cycling genes in agricultural soils: a meta-analysis of field studies. Soil Biol. Biochem. 127, 71–78. https://doi.org/10.1016/j.soilbio.2018.08.024.

Rabbani, M., Heidari, R., Yazdanparast, R., 2019. A stochastic multi-period industrial hazardous waste location-routing problem: integrating NSGA-II and Monte Carlo simulation. Eur. J. Oper. Res. 272, 945–961. https://doi.org/10.1016/j.ejor.2018.07.024.

Shen, H., Huang, Y., Wang, R., Zhu, D., Li, W., Shen, G., Wang, B., Zhang, Y., Chen, Y., Lu, Y., Chen, H., Li, T., Sun, K., Li, B., Liu, W., Liu, J., Tao, S., 2013. Global atmospheric emissions of polycyclic aromatic hydrocarbons from 1960 to 2008 and future predictions. Environ. Sci. Technol. 47, 6415–6424. https://doi.org/10.1021/es400857z.

Song, S., Zhang, C., Gao, Y., Zhu, X., Wang, R., Wang, M., Zheng, Y., Hou, L., Liu, M., Wu, D., 2020. Responses of wetland soil bacterial community and edaphic factors to two-year experimental warming and Spartina alterniflora invasion in Chongming Island. J. Clean. Prod. 250, 119502 https://doi.org/10.1016/j.jclepro.2019.119502.

Song, Y., Xue, C., Zhang, Y., Liu, P., Bao, F., Li, X., Mu, Y., 2023. Measurement report: exchange fluxes of HONO over agricultural fields in the North China Plain. EGUsphere 2023, 1–38. https://doi.org/10.5194/egusphere-2023-1223.

Sörgel, M., Trebs, I., Serafimovich, A., Moravek, A., Held, A., Zetzsch, C., 2011. Simultaneous HONO measurements in and above a forest canopy: influence of turbulent exchange on mixing ratio differences. Atmos. Chem. Phys. 11, 841–855. https://doi.org/10.5194/acp-11-841-2011.

Su, H., Cheng, Y., Oswald, R., Behrendt, T., Trebs, I., Meixner, F.X., Andreae, M.O., Cheng, P., Zhang, Y., Pöschl, U., 2011. Soil nitrite as a source of atmospheric HONO and OH radicals. Science 333, 1616–1618. https://doi.org/10.1126/science.1207687.

Sun, L., Chen, T., Jiang, Y., Zhou, Y., Sheng, L., Lin, J., Li, J., Dong, C., Wang, C., Wang, X., Zhang, Q., Wang, W., Xue, L., 2020. Ship emission of nitrous acid (HONO) and its impacts on the marine atmospheric oxidation chemistry. Sci. Total Environ. 735, 139355 https://doi.org/10.1016/j.scitotenv.2020.139355.

Tang, K., Qin, M., Duan, J., Fang, W., Meng, F., Liang, S., Xie, P., Liu, J., Liu, W., Xue, C., Mu, Y., 2019. A dual dynamic chamber system based on IBBCEAS for measuring fluxes of nitrous acid in agricultural fields in the North China Plain. Atmos. Environ. 196, 10–19. https://doi.org/10.1016/j.atmosenv.2018.09.059.

Van Dijk, S.M., Gut, A., Kirkman, G.A., Gomes, B.M., Meixner, F.X., Andreae, M.O., 2002. Biogenic NO emissions from forest and pasture soils: relating laboratory studies to field measurements. J. Geophys. Res. 107 https://doi.org/10.1029/2001JD000358.

Veres, P., Roberts, J.M., Burling, I.R., Warneke, C., De Gouw, J., Yokelson, R.J., 2010. Measurements of gas-phase inorganic and organic acids from biomass fires by negative-ion proton-transfer chemical-ionization mass spectrometry. J. Geophys. Res. 115, D23302 https://doi.org/10.1029/2010JD014033.

Wang, J., Wang, G., Wu, C., Li, Jianjun, Cao, C., Li, Jin, Xie, Y., Ge, S., Chen, J., Zeng, L., Zhu, T., Zhang, R., Kawamura, K., 2020. Enhanced aqueous-phase formation of secondary organic aerosols due to the regional biomass burning over North China Plain. Environ. Pollut. 256, 113401 https://doi.org/10.1016/j.envpol.2019.113401.

Wang, Y., Fu, X., Wang, T., Ma, J., Gao, H., Wang, X., Pu, W., 2023. Large contribution of nitrous acid to soil-emitted reactive oxidized nitrogen and its effect on air quality. Environ. Sci. Technol. 57, 3516–3526. https://doi.org/10.1021/acs.est.2c07793.

Wang, Y., Fu, X., Wu, D., Wang, M., Lu, K., Mu, Y., Liu, Z., Zhang, Y., Wang, T., 2021. Agricultural fertilization aggravates air pollution by stimulating soil nitrous acid emissions at high soil moisture. Environ. Sci. Technol. 55, 14556–14566. https://doi.org/10.1021/acs.est.1c04134.

Weber, B., Wu, D., Tamm, A., Ruckteschler, N., Rodríguez-Caballero, E., Steinkamp, J., Meusel, H., Elbert, W., Behrendt, T., Sörgel, M., Cheng, Y., Crutzen, P.J., Su, H., Pöschl, U., 2015. Biological soil crusts accelerate the nitrogen cycle through large NO and HONO emissions in drylands. Proc. Natl. Acad. Sci. U.S.A. 112, 15384–15389. https://doi.org/10.1073/pnas.1515818112.

Wu, D., Horn, M.A., Behrendt, T., Müller, S., Li, J., Cole, J.A., Xie, B., Ju, X., Li, G., Ermel, M., Oswald, R., Fröhlich-Nowoisky, J., Hoor, P., Hu, C., Liu, M., Andreae, M. O., Pöschl, U., Cheng, Y., Su, H., Trebs, I., Weber, B., Sörgel, M., 2019. Soil HONO emissions at high moisture content are driven by microbial nitrate reduction to nitrite: tackling the HONO puzzle. ISME J. 13, 1688–1699. https://doi.org/10.1038/s41396-019-0379-y.

Wu, D., Zhang, J., Wang, M., An, J., Wang, Ruhai, Haider, H., Xu-Ri, Huang, Y., Zhang, Q., Zhou, F., Tian, H., Zhang, X., Deng, L., Pan, Y., Chen, X., Yu, Y., Hu, C., Wang, Rui, Song, Y., Gao, Z., Wang, Y., Hou, L., Liu, M., 2022. Global and regional patterns of soil nitrous acid emissions and their acceleration of rural photochemical reactions. JGR Atmospheres 127. https://doi.org/10.1029/2021JD036379.

Wu, R., Xie, S., 2017. Spatial distribution of ozone formation in China derived from emissions of speciated volatile organic compounds. Environ. Sci. Technol. 51, 2574–2583. https://doi.org/10.1021/acs.est.6b03634.

Xu, Z., Wang, T., Wu, J., Xue, L., Chan, J., Zha, Q., Zhou, S., Louie, P.K.K., Luk, C.W.Y., 2015. Nitrous acid (HONO) in a polluted subtropical atmosphere: seasonal variability, direct vehicle emissions and heterogeneous production at ground surface. Atmos. Environ. 106, 100–109. https://doi.org/10.1016/j.atmosenv.2015.01.061.

Xue, C., Ye, C., Zhang, C., Catoire, V., Liu, P., Gu, R., Zhang, J., Ma, Z., Zhao, X., Zhang, W., Ren, Y., Krysztofiak, G., Tong, S., Xue, L., An, J., Ge, M., Mellouki, A., Mu, Y., 2021. Evidence for strong HONO emission from fertilized agricultural fields and its remarkable impact on regional O_3 pollution in the summer North China Plain. ACS Earth Space Chem. 5, 340–347. https://doi.org/10.1021/acsearthspacechem.0c00314.

Xue, C., Ye, C., Zhang, Y., Ma, Z., Liu, P., Zhang, C., Zhao, X., Liu, J., Mu, Y., 2019. Development and application of a twin open-top chambers method to measure soil HONO emission in the North China Plain. Sci. Total Environ. 659, 621–631. https://doi.org/10.1016/j.scitotenv.2018.12.245.

Xue, C., Zhang, Chenglong, Ye, C., Liu, P., Catoire, V., Krysztofiak, G., Chen, H., Ren, Y., Zhao, X., Wang, J., Zhang, F., Zhang, Chongxu, Zhang, J., An, J., Wang, T., Chen, J., Kleffmann, J., Mellouki, A., Mu, Y., 2020. HONO budget and its role in nitrate formation in the rural North China Plain. Environ. Sci. Technol. 54, 11048–11057. https://doi.org/10.1021/acs.est.0c01832.

Yang, Y., Li, X., Zu, K., Lian, C., Chen, S., Dong, H., Feng, M., Liu, H., Liu, J., Lu, K., Lu, S., Ma, X., Song, D., Wang, W., Yang, S., Yang, X., Yu, X., Zhu, Y., Zeng, L., Tan, Q., Zhang, Y., 2021. Elucidating the effect of HONO on O3 pollution by a case study in southwest China. Sci. Total Environ. 756, 144127 https://doi.org/10.1016/j.scitotenv.2020.144127.

Yienger, J.J., Levy, H., 1995. Empirical model of global soil-biogenic NO_x emissions. J. Geophys. Res. 100, 11447 https://doi.org/10.1029/95JD00370.

Yin, X., Tang, F., Huang, Z., Liao, S., Sha, Q., Cheng, P., Lu, M., Li, Z., Yu, F., Xu, Y., Shao, M., Zheng, J., 2023. Developing a model-ready highly resolved HONO emission inventory in Guangdong using domestic measured emission factors. Sci. Total Environ. 899, 165737 https://doi.org/10.1016/j.scitotenv.2023.165737.

Zhang, J., An, J., Qu, Y., Liu, X., Chen, Y., 2019. Impacts of potential HONO sources on the concentrations of oxidants and secondary organic aerosols in the Beijing-Tianjin-Hebei region of China. Sci. Total Environ. 647, 836–852. https://doi.org/10.1016/j.scitotenv.2018.08.030.

Zhang, J., Lian, C., Wang, W., Ge, M., Guo, Y., Ran, H., Zhang, Y., Zheng, F., Fan, X., Yan, C., Daellenbach, K.R., Liu, Y., Kulmala, M., An, J., 2022. Amplified role of potential HONO sources in O_3 formation in North China Plain during autumn haze aggravating processes. Atmos. Chem. Phys. 22, 3275–3302. https://doi.org/10.5194/acp-22-3275-2022.

Zhang, L., Wang, T., Zhang, Q., Zheng, J., Xu, Z., Lv, M., 2016. Potential sources of nitrous acid (HONO) and their impacts on ozone: a WRF-Chem study in a polluted subtropical region: modeling HONO IN a subtropical region. J. Geophys. Res. Atmos. 121, 3645–3662. https://doi.org/10.1002/2015JD024468.

Zhao, Y., Li, B., Dong, J., Li, Y., Wang, X., Gan, C., Lin, Y., Liao, H., 2023. Improved ammonia emission inventory of fertilizer application for three major crops in China based on phenological data. Sci. Total Environ. 896, 165225 https://doi.org/10.1016/j.scitotenv.2023.165225.